Effect of substrate on the microstructure and thermoelectric performances of Sr-doped $Ca_3Co_4O_9$ thick films

M. A. Torres, M. Mora*, H. Amaveda, M. A. Madre, A. Sotelo

ICMA (CSIC-Universidad de Zaragoza), C/María de Luna 3, 50018-Zaragoza (Spain).

Abstract

$Ca_3Co_4O_9$ thermoelectric materials in form of thick films are very promising in practical applications due to their low costs and relatively high performance. In this work, two different suspensions have been used to produce different coatings on Al_2O_3 polycrystalline substrates with theoretical green thickness of 360 and 2000 μm. Moreover, the effect of substrate has also been investigated using Al_2O_3 monocrystalline substrates and a 360 μm green thickness. Sintering procedure at 900 ºC for 24 h has drastically decreased coating thickness. XRD performed on the coatings surface has shown the formation of small amounts of $Ca_3Co_2O_6$ secondary phase on the polycrystalline substrates, while it was more abundant, and accompanied by $Ca_2Co_2O_5$ on the monocrystalline substrates. In spite of the higher secondary phases content, monocrystalline substrates produced a slight grain orientation which led to the highest thermoelectric properties between the samples (0.38 mW/K^2m at 800 ºC), and very close to the best reported values in the literature.

Keywords: Ceramics; Oxides; Thick films; Microstructure; Electrical properties; Thermoelectrics

* Corresponding author: M. Mora (mmora@unizar.es). ICMA (CSIC-Universidad de Zaragoza), C/María de Luna 3, 50018-Zaragoza (Spain). Tel.: +34 976762617

1. Introduction

Last years, fossil fuels consumption, after a decrease associated to the economic crisis, has started to grow again. Consequently, the emissions of CO_2 and greenhouse gases have been drastically raised. Taking into account that their main use is producing energy and that the efficiency of such systems is low, a large amount of the original energy is lost in form of heat. Consequently, thermoelectric (TE) materials, which are able to harvest this wasted heat transforming it into electric power [1], can increase the efficiency of these energy transforming systems. In addition, the energy consumption can be decreased, with the corresponding reduction of emissions. For this purpose, efficient heat conversion materials are necessary, usually in terms of the so-called dimensionless figure-of-merit, described as:

$$ZT = \frac{S^2 T}{\rho \kappa}$$

where Seebeck coefficient (S), absolute temperature (T), electrical resistivity (ρ), and thermal conductivity (κ), parameters are involved [2].

Even if TE materials are known for long time [3], they are scarcely used in energy harvesting applications. Nowadays, the most important applications of TE materials are limited to intermetallic ones (as $CoSb_3$ or Bi_2Te_3 [4,5]) in climate control field. On the other hand, for power applications their working temperature is usually low, with problems associated to release of heavy metals or degradation, both induced by high temperatures [1]. In 1997, ceramic materials ($Na_2Co_2O_4$ [6]) were discovered to have good TE performances, together with the ability to work at high temperature, the absence of heavy metals, and their more environmentally friendly behavior. An additional advantage is that the elements forming these ceramics are more abundant in

earth's crust [7]. From this moment, the intense work performed on TE ceramics allowed the improvement of different materials, such as CoO-, TiO-, MnO-, or FeO-based families [8-11]. Among the members of the first family, the $Ca_3Co_4O_9$ (349) material, without any heavy metal in its composition, possess relatively high TE properties. Moreover, an economic and strategic advantage is that the raw compounds are abundant and low cost. On the other hand, its drawback can be summarized in the anisotropic electric properties induced by its crystal structure [8], and the difficult densification due to the large temperature difference between the eutectic point and the stability range of 349 phase [12]. Consequently, many efforts have been made to enhance structural, microstructural, and thermoelectric properties of this material, as grain alignment [13], doping [14], synthesis [15], or other non-conventional methods [16,17].

Other possibility to further reduce the costs associated to the fabrication processes is the use of thick films which, besides their low costs, offer the possibility of automatic large scale production. Moreover, the production technology of thick films is well-known, while their reliability has been proved for long time in hybrid circuits and silicon solar cells [18] and, more recently, in thermoelectric materials [19,20].

The objective of this work is the fabrication of thermoelectric thick films of $Ca_3Co_4O_9$ materials with improved performances via Sr-doping [21,22], and prepared through dip coating technique [23], which is a simple and low cost method that allows obtaining high quality coatings. Sr-doping is well known to produce $Ca_3Co_4O_9$ materials with S values higher than the obtained in pure $Ca_3Co_4O_9$ samples at high temperatures, due to the modification of misfit parameter associated to the large size of Sr^{2+}, compared to Ca^{2+}

[24]. The structural, and microstructural evolution of different thick films will be studied after sintering and correlated with the thermoelectric performances.

2. Experimental

Some works performed on the improvement of thermoelectric performances of 349 phase via doping, have demonstrated that isovalent substitutions (Ca by Sr) enhance electric transport properties [21,22]. Hence, $Ca_{2.93}Sr_{0.07}Co_4O_9$ initial nominal stoichiometry has been selected. Initial mixture has been prepared using $CaCO_3$ (≥ 99 %, Aldrich), $SrCO_3$ (≥ 98%, Aldrich), and CoO (99.99 %, Aldrich) commercial powders as raw materials. The stoichiometric amouns of each compound were weighed and attrition milled in water media with ZrO_2 balls for 30 min, followed by sieving to separate the grinding media. Water was then evaporated using infrared lamps to obtain a homogeneous mixture composed of very small grains [15]. After manual milling, the powders were mixed with a deffloculant (Hypermer KD1) and a fixed volume of azeotropic mixture of Methyl ethyl ketone (MEK)/ethanol in a planetary ball mill for 4 h at 350 rpm in alumina media. Binder (Polyvinyl Butyral B79) and plasticizers (Dibutyl Phthalate, and Polyalkylene Glycol) were added to the resulting suspension, followed by ball milling for 2 h using polycarbonate grinding balls. Finally, the mixture was degassed and stirred with a magnetic stirrer for about 24 h to homogenize the suspension. Several suspensions using different solid contents were prepared for coating polycrystalline Al_2O_3 substrates. They were dipped into the different ceramic suspensions and coated with a withdrawal speed of 15 mm/s. The as-deposited films were drying at ambient temperature for 24 hours. Before immersion, the substrates

were cleaned by sonication, and submerged sequentially in a dilute acid solution, water and ketone for several minutes. Moreover, in order to study the possible effect of substrate on the structural, microstructural and thermoelectric properties of the sintered materials, monocrystalline substrates were also coated using the lowest solid containing suspension, previously determined, to clearly observe the substrate effect on the final products.

Once the coating were totally dried, they were subjected to a two-step thermal treatment at 450 ºC for 2 h to decompose the organic material, followed by heating at 900 ºC for 24 h, under air, with a final furnace cooling. Sintered coatings were structurally characterized through XRD performed on their surfaces in a PANalytical X'Pert MPD Philips diffractometer (CuKα radiation) between 5 and 40 degrees. Microstructure has been studied on transversal surfaces using a Field Emission Scanning Electron Microscope (FESEM, Zeiss Merlin) equipped with an energy dispersive spectrometry (EDS) analysis system. Electrical properties (electrical resistivity, and Seebeck coefficient) were determined through the standard four-probe DC technique between 50 and 800 ºC, under He, in a LSR-3 system (Linseis GmbH). Finally, TE performances of coatings were obtained by calculating their power factor, PF (= S^2/ρ).

The samples will be hereafter named as P1 for the polycrystalline substrates coated with the lowest solid content, P2 for the ones with the highest solid content, and M1 for the monocrystalline substrates.

3. Results and discussion

The batch formulation of ceramic slurries used in this study is given by table 1. Only two suspensions, with 22, and 29 vol.% solid content have been studied, taking into account the expected green coating thickness. Their viscosity curves show shear-thinning flow behaviour in the shear region from 1 s^{-1} to 1000 s^{-1}, which is typical one for weakly flocculated suspensions. This is very beneficial for obtaining homogeneous films because during the coating process the suspension will show lower viscosity, while during the evaporation process it will show increased viscosity, which prevents movement of the particles and sedimentation thereof.

The thickness of the resulting coatings has been estimated from [23] using the values of powder density (4,67 g/cm^3), the surface tension (~ 22mN/m), viscosity of the suspension at 100 s^{-1} (0,6 and 9 Pas for suspension with lower and higher solid content, respectively), as well as the withdrawal speed, being around 360 and 2000 μm, respectively. Moreover, no differences in adhesion of films to the different substrates have been found after sintering procedure.

XRD patterns performed on the sintered films surfaces are shown in Fig. 1. In a first sight, it is clear that major peaks are associated to the $Ca_3Co_4O_9$–based phase (identified by their diffraction planes) [25]. Moreover, no Sr-rich secondary phases are identified, indicating that Sr is incorporated in the crystal structure, in agreement with previous works [21,22]. On the other hand, large difference can be observed between the samples sintered on monocrystalline and polycrystalline substrates, with much higher $Ca_3Co_2O_6$ phase content [25] in samples sintered on monocrystalline substrates. Furthermore, the higher relative intensity of (004) reflection, compared with the (002) one in M1 samples, indicates the formation of another secondary phase, $Ca_2Co_2O_5$ [26].

These results clearly point out to a remarkable effect of substrate on the phases evolution despite of the relatively low temperature used for sintering, when compared with the necessary to produce a liquid phase [12].

Microstructural observations of transversal sections of samples have shown that their thickness is very homogeneous all along the samples, with values of 55.67 $\pm$ 2.10 μm for samples P1, 39.41 $\pm$ 2.09 μm for M1, and 272.56 $\pm$ 20.15 μm for P2 ones. These data clearly illustrates that a moderate change on the solid content (from 22 to 29 vol.%) produces a drastic modification on the coating thickness (from 55.97 to 272.56 μm). Furthermore, it can be also deduced that monocrystalline substrates lead to higher densification than the polycrystalline ones. This evolution is illustrated in Fig. 2, where representative micrographs of all samples are presented. In the micrographs, it can be observed that grain sizes and porosity content are increased from M1 to P2. Moreover, only M1 samples seem to have a slight grain alignment, when compared with the P1 and P2 ones. On the other hand, EDS analysis has shown the presence of $Ca_3Co_2O_6$ phase in all samples, being in much higher proportion in M1 samples, in agreement with the XRD patterns previously discussed. This is also clear evidence that the substrate can play an important role on the final microstructure of sintered $Ca_3Co_4O_9$ coatings.

Electrical resistivity measurements, as a function of temperature, performed in all samples, are presented in Fig. 3. In the graph, it can be observed that all samples show semiconducting-like behavior in the whole measured temperature range, in agreement with previous works [16,27]; however, it is much less evident for M1 samples. Moreover, in spite of their higher content in $Ca_3Co_2O_6$ secondary phase, M1 samples display the lowest electrical resistivity among all samples, while S1 ones possess the highest ones.

This evolution can be explained taking into account several factors influencing electrical resistivity, such as grain sizes and orientation, porosity, and secondary phases content, previously discussed in XRD and SEM sections. In these images it was observed that M1 samples, in spite of the smaller grain sizes and higher secondary phase content, showed the lowest porosity, and a slight grain orientation, when compared with the other samples. Between P1, and P2, the last one possesses larger grain sizes, while the other parameters are approximately the same for both kind of samples, explaining the lower resistivity of P2 samples, compared with P1 one. Furthermore, this evolution is in clear agreement with previous works which showed that grain orientation possesses higher influence on electrical resistivity than secondary phases content [28]. The lowest ρ values at 800 ºC (8.2 mΩ.cm) determined on M1 samples is much lower than the measured in sintered materials (40 mΩ.cm) [13], and close to the obtained in highly textured materials through hot-pressing (6.9 mΩ.cm) [13], or edge free spark plasma sintering (SPS, 7 mΩ.cm) [29]. This is a clear evidence of the formation of strong links between grains induced by the monocrystalline substrate.

Fig. 4 shows the variation of the Seebeck coefficient with temperature in all samples. The measured S values are positive for all samples, indicating that major charge carriers are holes. Moreover, the S values are increased when the temperature is raised, with very similar behavior for P1, and P2 samples, confirming that the substrate influences the properties of sintered coatings, and that the amount of solid in the initial suspension has a negligible effect on the S values. When evaluating the maximum S values at 800 ºC (212 μV/K) measured in P1 samples, they are higher than the

measured in sintered materials (180-190 μV/K) [13,27], and highly textured materials through hot-pressing (170 μV/K) [13], or SPS (165 μV/K) [29].

The temperature dependence of PF, calculated from the electrical resistivity and Seebeck coefficient data, is presented in Fig. 5. PF increases with temperature, showing the opposite evolution, between samples, observed in the electrical resistivity. The highest PF values have been obtained in M1 samples in the whole measured temperature range, reaching 0.38 mW/K^{2}m at 800 ºC, which are very close to the best ones reported in the literature (around 0.43 mW/K^{2}m) [29-32].

From all these data, it is clear that the use of monocrystalline Al_2O_3 substrates is beneficial to produce high performance $Ca_3Co_4O_9$ sintered coatings using the dip-coating technique. Still, it is necessary to optimize the sintering procedure for this substrate in order to minimize the amount of $Ca_3Co_2O_6$ phase, maximizing its TE performances.

4. Conclusions

$Ca_3Co_4O_9$ thermoelectric thick films have been successfully prepared on Al_2O_3 polycrystalline and monocrystalline substrates through the dip-coating technique. XRD analysis has shown that $Ca_3Co_4O_9$ phase is the major one in all cases. However, monocrystalline substrates have led to higher content of $Ca_3Co_2O_6$ secondary phase than in the polycrystalline ones. Moreover, a new secondary phase, $Ca_2Co_2O_5$, has also been identified in the monocrystalline substrates. SEM observation showed that monocrystalline substrates drastically decrease the coating thickness after sintering and provides a slight grain orientation. These characteristics are reflected on the electrical

resistivity that, in spite of their higher secondary phases content, is much lower in the monocrystalline substrates than in the polycrystalline ones, due to their slight grain orientation. On the other hand, their Seebeck coefficient is lower than in the polycrystalline substrates, in agreement with their lower resistivity. The maximum power factor values, 0.38 mW/K^{2}m at 800 ºC measured in the monocrystalline substrates is very close to the best ones reported in the literature. These data clearly indicate that higher PF values can be obtained in further studies to decrease the amount of secondary phases in the monocrystalline substrate.

Acknowledgements

The authors wish to thank the Gobierno de Aragón-FEDER (Research Group T 54-17R), and the Spanish MINECO-FEDER (Project MAT2017-82183-C3-1-R) for financial support. Authors would like to acknowledge the use of Servicio General de Apoyo a la Investigación-SAI, Universidad de Zaragoza.

References

[1] M.H. Elsheikh, D.A. Shnawah, M.F.M. Sabri, S.B.M. Said, M.H. Hassan, M.B.A. Bashir, M. Mohamad, A review on thermoelectric renewable energy: Principle parameters that affect their performance, Renew. Sustain. Energy Rev. 30 (2014) 337-355.

[2] D.M. Rowe, D.M. Rowe (Ed.), Thermoelectrics Handbook: Macro to Nano, 1st ed., CRC Press, Boca Raton, FL, 2006, pp. 1-3–1-7.

[3] T.J. Seebeck, Magnetic polarization of metals and minerals, Abhandlungen der Deutschen Akademie der Wissenschafren zu Berlin, 265, (1822-1823).

[4] J.A. Santamaria, J. Alkorta, J.G. Sevillano, Microcompression tests of single-crystalline and ultrafine grain Bi_2Te_3 thermoelectric material, J. Mater. Res. 30 (2015) 2593-2604.

[5] H. Wang, J. Hwang, M.L. Snedaker, I.-H. Kim, C. Kang, J. Kim, G.D. Stucky, J. Bowers, W. Kim, High Thermoelectric Performance of a Heterogeneous PbTe Nanocomposite, Chem. Mater. 27 (2015) 944-949.

[6] I. Terasaki, Y. Sasago, K. Uchinokura, Large thermoelectric power in $NaCo_2O_4$ single crystals, Phys. Rev. B 56 (1997) 12685-12687.

[7] A.A. Yaroshevsky, Abundances of Chemical Elements in the Earth's Crust, Geochem. Int. 44 (2006) 48-55.

[8] A.C. Masset, C. Michel, A. Maignan, M. Hervieu, O. Toulemonde, F. Studer, B. Raveau, J. Hejtmanek, Misfit-layered cobaltite with an anisotropic giant magnetoresistance: $Ca_3Co_4O_9$, Phys. Rev. B 62 (2000) 166-175.

[9] H. Wang, C.L. Wang, Thermoelectric properties of Yb-doped $La_{0.1}Sr_{0.9}TiO_3$ ceramics at high temperature, Ceram. Int. 39 (2013) 941-946.

[10] Y.H. Zhu, W.B. Su, J. Liu, Y.C. Zhou, J.C. Li, X.H. Zhang, Y.L. Du, C.L. Wang, Effects of Dy and Yb co-doping on thermoelectric properties of $CaMnO_3$ ceramics, Ceram. Int. 41 (2015) 1535-1539.

[11] N.M. Ferreira, F.M. Costa, A.V. Kovalevsky, M.A. Madre, M.A. Torres, J.C. Diez, A. Sotelo, New environmentally friendly Ba-Fe-O thermoelectric material by flexible laser floating zone processing, Scr. Mater. 145 (2018) 54-57.

[12] D. Sedmidubsky, V. Jakes, O. Jankovsky, J. Leitner, Z. Sofer, J. Hejtmanek, Phase equilibria in Ca-Co-O system, J. Solid State Chem. 194 (2012) 199-205.

[13] H. Wang, X. Sun, X. Yan, D. Huo, X. Li, J.-G. Li, X. Ding, Fabrication and thermoelectric properties of highly textured $Ca_9Co_{12}O_{28}$ ceramic, J. Alloys Compds. 582 (2014) 294-298.

[14] N. Prasoetsopha, S. Pinitsoontorn, T. Kamwanna, V. Amornkitbamrung, K. Kurosaki, Y. Ohishi, H. Muta, S. Yamanaka, The effect of Cr substitution on the structure and properties of misfit-layered $Ca_3Co_{4-x}Cr_xO_{9+\delta}$ thermoelectric oxides, J. Alloys Compds. 588 (2014) 199-205.

[15] A. Sotelo, Sh. Rasekh, M.A. Torres, P. Bosque, M.A. Madre, J.C. Diez, Effect of synthesis methods on the $Ca_3Co_4O_9$ thermoelectric ceramic performances, J. Solid State Chem. 221 (2015) 247-254.

[16] T. Schulz, J. Topfer, Thermoelectric properties of $Ca_3Co_4O_9$ ceramics prepared by an alternative pressure-less sintering/annealing method, J. Alloys Compds. 659 (2016) 122-126.

[17] A. Sotelo, F.M. Costa, N.M. Ferreira, A. Kovalevsky, M.C. Ferro, V.S. Amaral, J.S. Amaral, Sh. Rasekh, M.A. Torres, M.A. Madre, J.C. Diez, Tailoring $Ca_3Co_4O_9$ microstructure and performances using a transient liquid phase sintering additive, J. Eur. Ceram. Soc. 36 (2016) 1025-1032.

[18] G.C.Dubey, Application of thick film techniques to the manufacture of solar cells, Solar Cells 15 (1985) 1-25.

[19] T. Schulz, T. Reimann, A. Bochmann, A. Vogel, B. Capraro, B. Mieller, S. Teichert, J. Topfer, Sintering behavior, microstructure and thermoelectric properties of calcium cobaltite thick films for transversal thermoelectric multilayer generators, J. Eur. Ceram. Soc. 38 (2018) 1600-1607.

[20] W.-H. Yoon, J. Ryu, J.-J. Choi, B.-D. Hahn, J.H. Choi, B.-K. Lee, J.-H. Cho, D.-S. Park, Enhanced Thermoelectric Properties of Textured $Ca_3Co_4O_9$ Thick Film by Aerosol Deposition, J. Am. Ceram. Soc. 93 (2010) 2125-2127.

[21] F. Delorme, C.F. Martin, P. Marudhachalam, D.O. Ovono, G. Guzman, Effect of Ca substitution by Sr on the thermoelectric properties of $Ca_3Co_4O_9$ ceramics, J. Alloys Compds. 509 (2011) 2311-2315.

[22] G. Constantinescu, Sh. Rasekh, M.A. Torres, J.C. Diez, M.A. Madre, A. Sotelo, Effect of Sr substitution for Ca on the $Ca_3Co_4O_9$ thermoelectric properties, J. Alloys Compds. 577 (2013) 511-515.

[23] T. Schneller, R. Waser, M. Kosec, D. Payne (Eds.), Chemical Solution Deposition of Functional Oxide Thin Films, Springer-Verlag, Wien, 2013.

[24] H. Yamauchi, L. Karvonen, T. Egashira, Y. Tanaka, M. Karppinen, Ca-for-Sr substitution in the thermoelectric $[(Sr,Ca)_2(O,OH)_2]_q[CoO_2]$ misfit-layered cobalt-oxide system, J. Solid State Chem. 184 (2011) 64–69.

[25] E. Woermann, A. Muan, Phase equilibria in the system CaO–cobalt oxide in air, J. Inorg. Nucl. Chem. 32 (1970) 1455-1459.

[26] J. Zhang, H. Zheng, C.D. Malliakas, J.M. Allred, Y. Ren, Q. Li, T.-H. Han, J.F. Mitchell, Brownmillerite $Ca_2Co_2O_5$: Synthesis, Stability, and Re-entrant Single Crystal to Single Crystal Structural Transitions, Chem. Mater. 26 (2014) 7172-7182.

[27] F. Delorme, P. Diaz-Chao, F. Giovannelli, Effect of Ca substitution by Fe on the thermoelectric properties of $Ca_3Co_4O_9$ ceramics, J. Electroceram. 40 (2018) 107-114.

[28] Sh. Rasekh, F.M. Costa, N.M. Ferreira, M.A. Torres, M.A. Madre, J.C. Diez, A. Sotelo, Use of laser technology to produce high thermoelectric performances in $Bi_2Sr_2Co_{1.8}O_x$, Mater. Design 75 (2015) 143-148.

[29] J.G. Noudem, D. Kenfaui, D. Chateigner, M. Gomina, Toward the enhancement of thermoelectric properties of lamellar $Ca_3Co_4O_9$ by edge-free spark plasma texturing, Scr. Mater. 66 (2012) 258-260.

[30] N.Y. Wu, T.C. Holgate, N.V. Nong, N. Pryds, S. Linderoth, High temperature thermoelectric properties of $Ca_3Co_4O_{9+\delta}$ by auto-combustion synthesis and spark plasma sintering, J. Eur. Ceram. Soc. 34 (2014) 925-931.

[31] J.G. Noudem, D. Kenfaui, D. Chateigner, M. Gomina, Granular and Lamellar Thermoelectric Oxides Consolidated by Spark Plasma Sintering, J. Electron. Mater. 40 (2011) 1100-1106.

[32] M.A. Madre, F.M. Costa, N.M. Ferreira, A. Sotelo, M.A. Torres, G. Constantinescu, Sh. Rasekh, J.C. Diez, Preparation of high-performance $Ca_3Co_4O_9$ thermoelectric ceramics produced by a new two-step method, J. Eur. Ceram. Soc. 33 (2013) 1747-1754.

Figure captions

Figure 1. Powder XRD patterns of different films surfaces after sintering on Al_2O_3 substrates: a) M1; b) P1; and b) P2. Peaks associated to $Ca_3Co_4O_9$ phase are shown by their diffraction planes, while * indicates the corresponding to the $Ca_3Co_2O_6$ one.

Figure 2. Representative SEM micrographs taken on longitudinal sections of $Ca_3Co_4O_9$ coatings on Al_2O_3 substrates: a) M1; b) P1; and c) P2.

Figure 3: Temperature dependence of the electrical resistivity for: ● M1; ■ P1; and ◆ P2 samples.

Figure 4: Temperature dependence of the Seebeck coefficient for: ● M1; ■ P1; and ◆ P2 samples.

Figure 5: Temperature dependence of power factor for: ● M1; ■ P1; and ◆ P2 samples.

Figure 1

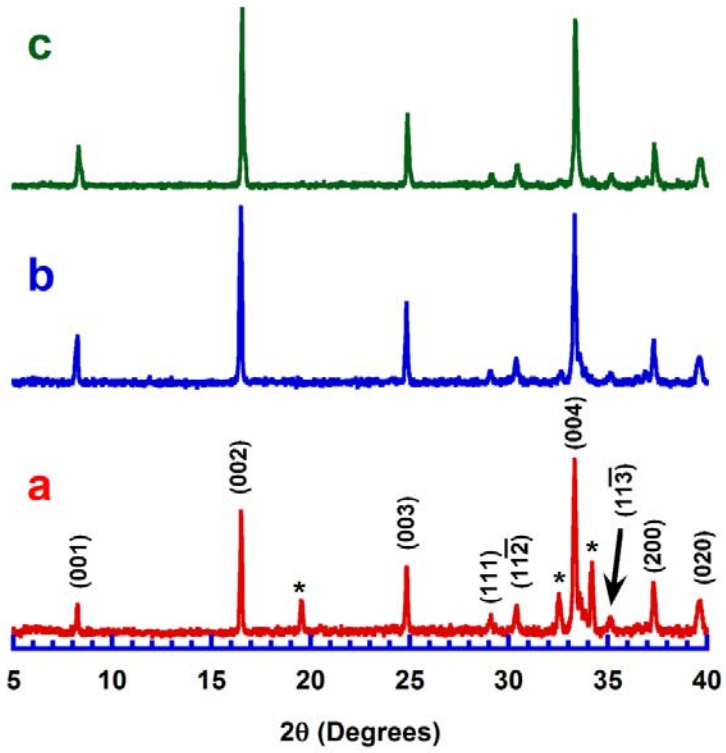
c
b
a
(001)
(002)
(003)
(111)
(11$\bar{2}$)
(004)
(11$\bar{3}$)
(200)
(020)
*
5
10
15
20
25
30
35
40
2θ (Degrees)

Figure 2

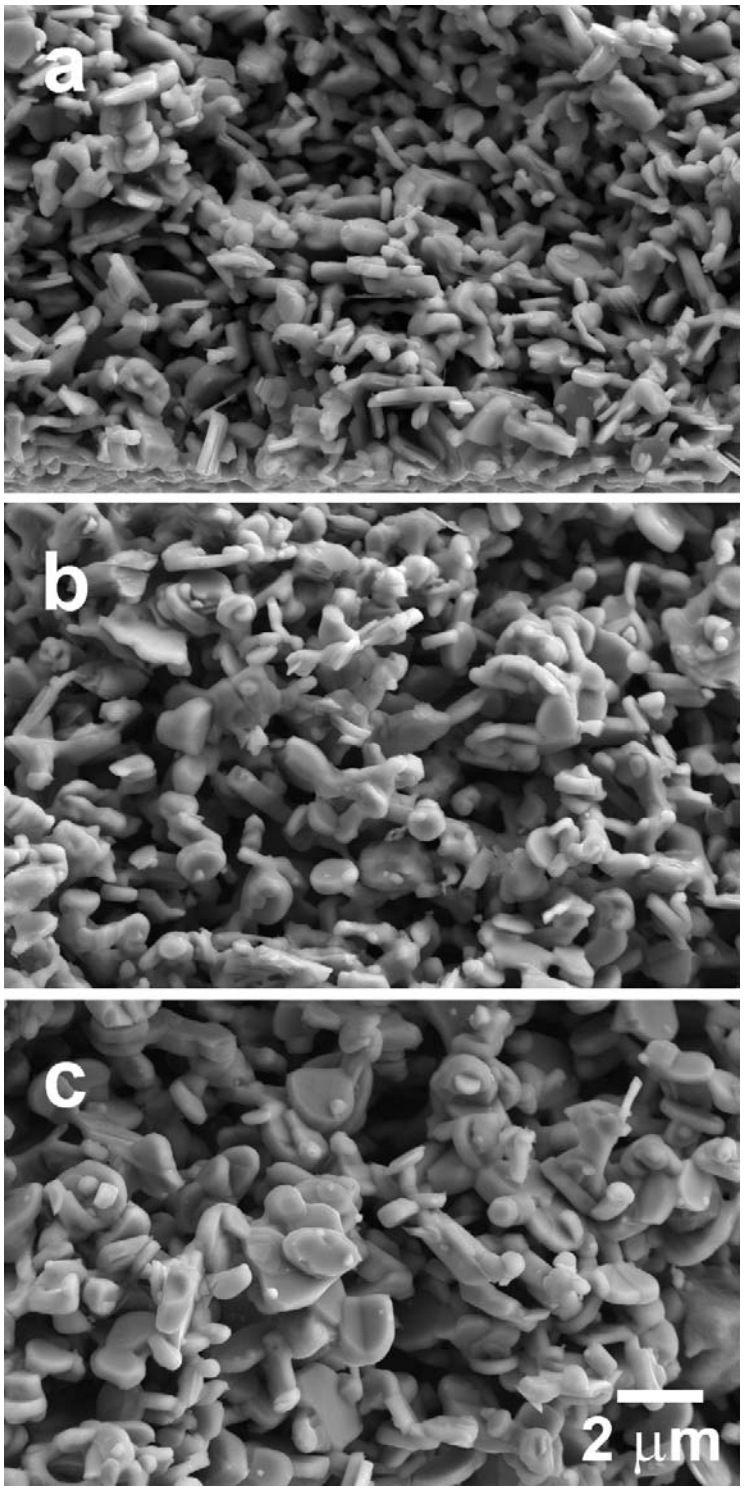

Figure 3

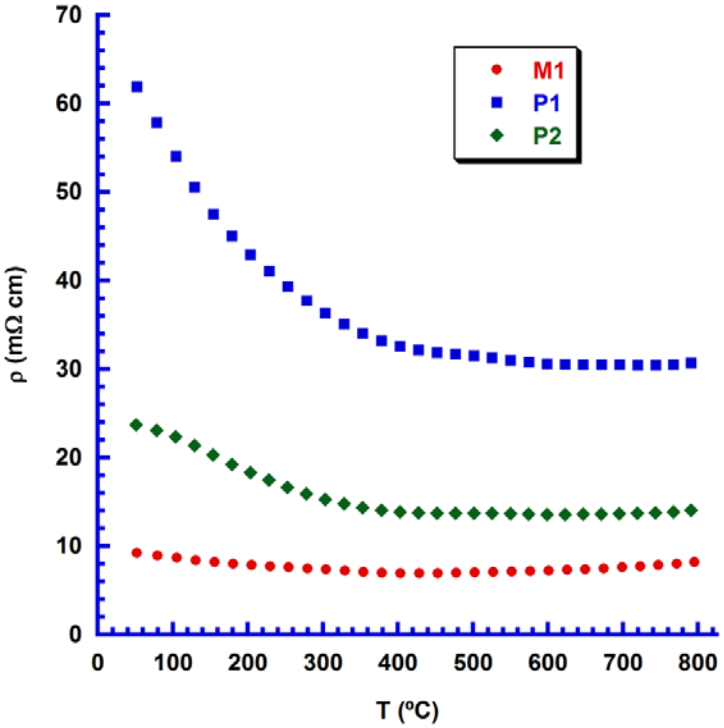
M1
P1
P2
ρ (mΩ cm)
T (ºC)
0
10
20
30
40
50
60
70
0
100
200
300
400
500
600
700
800

Figure 4

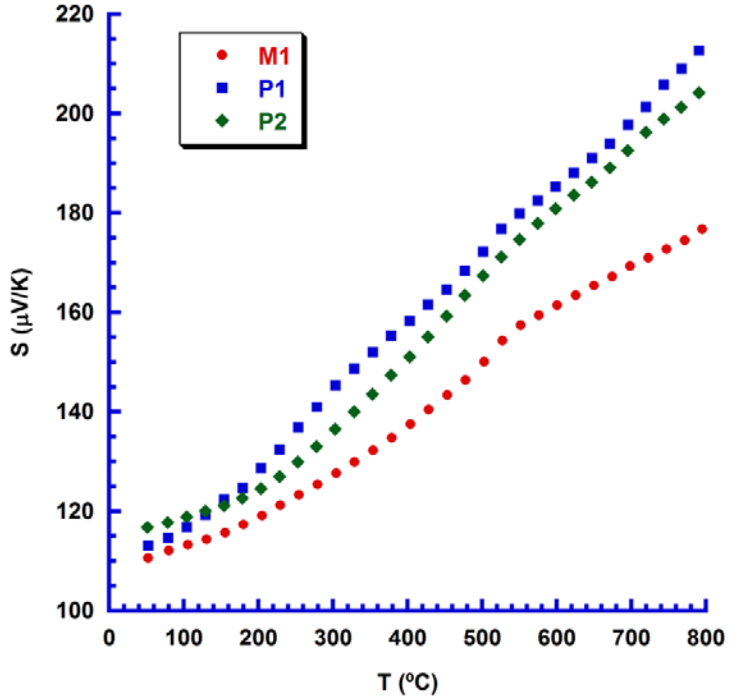
M1
P1
P2
S (μV/K)
T (°C)
220
200
180
160
140
120
100
0
100
200
300
400
500
600
700
800

Figure 5

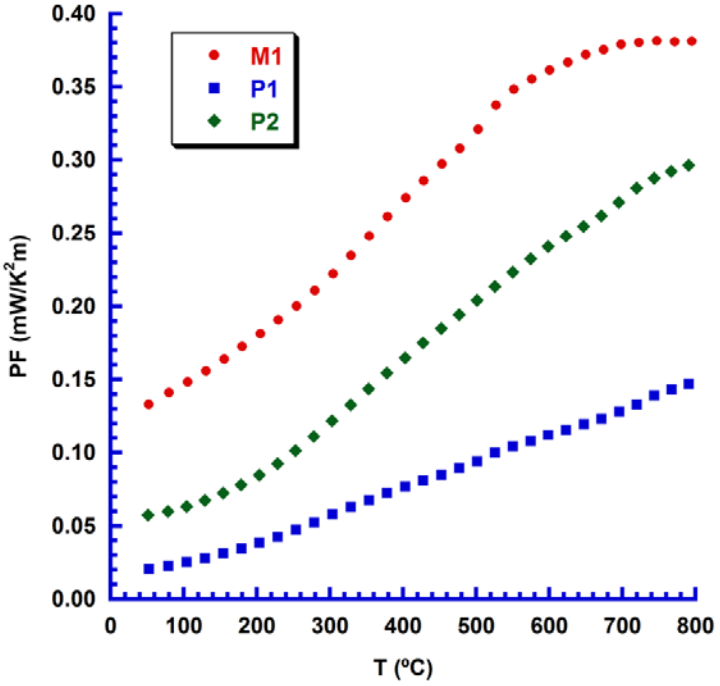
M1
P1
P2
PF (mW/K²m)
T (°C)
0.00
0.05
0.10
0.15
0.20
0.25
0.30
0.35
0.40
0
100
200
300
400
500
600
700
800